Scaling law for the Lyapunov spectra in globally coupled tent maps

Satoru Morita*
''Research for the Future'' Project, Faculty of Science and Technology, Keio University, Shin-Kawasaki-Mitsui Building West 3F, 890-12 Kashimada, Saiwai-ku, Kawasaki 211-0958, Japan
(Received 29 December 1997; revised manuscript received 11 March 1998)

The collective motions in globally coupled tent maps are investigated in terms of Lyapunov spectra. The scattered states are separated into two distinct phases by the characteristics of the Lyapunov spectra. In the weak-coupling phase, the Lyapunov spectra obey a scaling law with varying system size. This scaling law holds even in the strong-coupling phase except for the singular property of the largest Lyapunov exponent. The Lyapunov exponents are estimated theoretically by using the random field approximation. These approximate results reveal the relation between the Lyapunov exponents and the distribution of the elements. Furthermore, the features of the band structure in the distribution are explored. [S1063-651X(98)04910-1]

PACS number(s): 05.45.+b, 05.70.Ln, 82.40.Bj

I. INTRODUCTION

The coupled nonlinear systems are used as mathematical models to study complex phenomena of systems out of equilibrium in various fields, such as fluid dynamics, biological systems, chemical reactions, etc. When the elements of the coupled systems have chaotic dynamics, the dynamics of the full systems may be high-dimensional chaos. While the nature of low-dimensional chaos has been well known, the understanding of high-dimensional chaos is not yet sufficient. In the present paper, let us consider high-dimensional chaos in terms of the Lyapunov spectrum. The Lyapunov spectrum is a set of the Lyapunov exponents $(\lambda_0,\lambda_1,\ldots,\lambda_{N-1})$, where N is the dimension of the phase space and the Lyapunov exponents are put in order as $\lambda_i \geqslant \lambda_{i+1}$. The Lyapunov spectrum is a useful tool to study the structure of the phase space of high-dimensional chaotic systems [1–7].

In the present paper, one of the simplest models is investigated analytically. The model we use here is globally coupled maps (GCM) [8],

$$x_{t+1}(i)=(1-\epsilon)f(x_t(i))+\frac{\epsilon}{N}\sum_{i'=0}^{N-1} f(x_t(i')). \tag{1}$$

Here t represents a discrete time step, i the index of the elements $(i=0,1,2,\ldots,N-1)$, and ϵ the coupling strength. The one-dimensional map $f(x)$ gives the dynamics of the element. We consider here the tent map

$$f(x)=1-a|x|. \tag{2}$$

The gradient a satisfies $1<a\leqslant 2$ for elements to give rise to chaotic dynamics. The initial condition is such that the elements are uniformly distributed over in the interval $[-1,1]$. The variable x of each map is always bounded in the same interval. The model (1) is a mean-field version of the coupled map lattice (CML), which has been investigated as a model of spatiotemporal chaos in the short-range coupling limit [9]. The global coupling in the model (1) may be regarded as either an idealization of long-range coupling or an approximation to short-range coupling in high-dimensional lattices. It should be noted that the concept of space loses meaning for the global coupling.

One of the most prominent phenomena in GCM is a collective motion [10–23]. The collective motion is expressed in terms of a macroscopic variable that depends on the motions of all elements in the system. The collective motion has been studied extensively since Kaneko observed a coherent motion in globally coupled logistic maps [10]. As for globally coupled tent maps, the analysis in terms of the Frobenius-Perron operator suggested there exist several types of collective motions [16–20]. In particular, the periodic and quasiperiodic motions have been investigated. Similar coherent motions were observed also in coupled map lattices [24–26] and globally coupled oscillators [27–29]. As a macroscopic variable, we employ the mean field

$$h_t=\frac{1}{N}\sum_{i=0}^{N-1} f(x_t(i)). \tag{3}$$

Thus, the coupling term in Eq. (1) is the mean field. Accordingly, the motion of the ith element is described by the effective map that depends on time through the mean field as follows:

$$x_{t+1}(i)=F_t(x_t(i))\equiv(1-\epsilon)f(x_t(i))+\epsilon h_t. \tag{4}$$

The collective motion of the system is expressed by the evolution of the mean field.

The purpose of the present paper is to investigate the nature of the Lyapunov exponents and the collective motions. There exist weak-coupling and strong-coupling phases in the region where the completely synchronized state is unstable. Numerical calculation shows that the Lyapunov spectra obey a scaling law in the weak-coupling phase. Even in the strong-coupling phase, the scaling law is valid except for the singular property of the largest Lyapunov exponent. To explain the scaling law, we estimate the Lyapunov exponents theoretically by the random field approximation used in [30–32]. Theoretical calculation suggests that the weak-coupling and strong-coupling phases correspond to ''variance dominated'' and ''mean dominated'' phases in [31], respectively.

*Electronic address: morita@future.st.keio.ac.jp

This paper is organized as follows. In Sec. II, the features of globally coupled tent maps (1) are introduced. In Sec. III, the numerical calculation of the Lyapunov spectrum is presented to show the scaling law. In Sec. IV, we calculate the Lyapunov spectrum by using the random field approximation. Though the exact structure of the Lyapunov spectrum is not obtained, theoretical results agree qualitatively with the numerical calculation. A relation between the Lyapunov spectrum and the distribution of the elements is disclosed. The transition between the above two phases is explored in Sec. V. This transition is related to the creation and the extinction of two chaotic bands in the distribution of the elements. Section VI contains concluding remarks.

II. FEATURES OF GLOBALLY COUPLED TENT MAPS

In this section, some features of globally coupled tent maps (1) are presented. The globally coupled tent maps have no clustering state, while clustering states are often observed in other globally coupled systems [10]. Thus, the attractors of Eq. (1) are classified into completely synchronized or scattered states as follows.

In the completely synchronized state, where all elements always have an identical value, the motion of the mean field h_t obeys the one-dimensional map $x \mapsto f(x)$. This state is stable for $a(1-\epsilon)<1$. In the completely synchronized state, only the largest Lyapunov exponent λ_0 is positive and the others $\lambda_{i\geqslant 1}$ are negative. From simple algebra, we obtain $\lambda_0=\ln a$ and $\lambda_{i\geqslant 1}=\ln[a(1-\epsilon)]$. It should be noted that the largest Lyapunov exponent equals the Lyapunov exponent of the map $x \mapsto f(x)$, while the others equal the local-instability rate

$$\lambda_{\mathrm{local}} \equiv \ln[a(1-\epsilon)], \tag{5}$$

which is defined by the rate of exponential divergence of the difference of two nearby elements [33]. Here, the term ''local'' represents a property for the individual elements but not for a short time scale. It is a specific feature of globally coupled tent maps that the local-instability rate is a well-defined exponent independent of the time t and the element index i.

On the other hand, for $a(1-\epsilon)>1$, the completely synchronized state is unstable. Thus, the elements are scattered and behave chaotically in time. This state is called the scattered state in this paper. In the scattered state, the number of positive Lyapunov exponents is always N. Thus, there is a bifurcation where the dimension of the motion changes abruptly from 1 to N. The bifurcation occurs at $a(1-\epsilon)=1$, where the local-instability rate is marginal, i.e., $\lambda_{\mathrm{local}}=0$. The N positive Lyapunov exponents mean that the N elements are almost independent mutually. If it is assumed that N elements are completely independent mutually, the mean field is a constant value in the limit of large size on account of the law of large numbers when $a(1-\epsilon)>\sqrt{2}$. [When $2^{2^{-n+1}}<a(1-\epsilon)<2^{2^{-n}}$, the mean field has a 2^n-period motion.] However, the mean-field cannot be constant generally, except for the case with specific parametric values, even in the limit of large size [20]. Therefore, the motions of all elements have mutual correlation. The mean field has a complex motion that can be high-dimensional chaos. In Fig. 1, we show examples of the motion of the mean field.

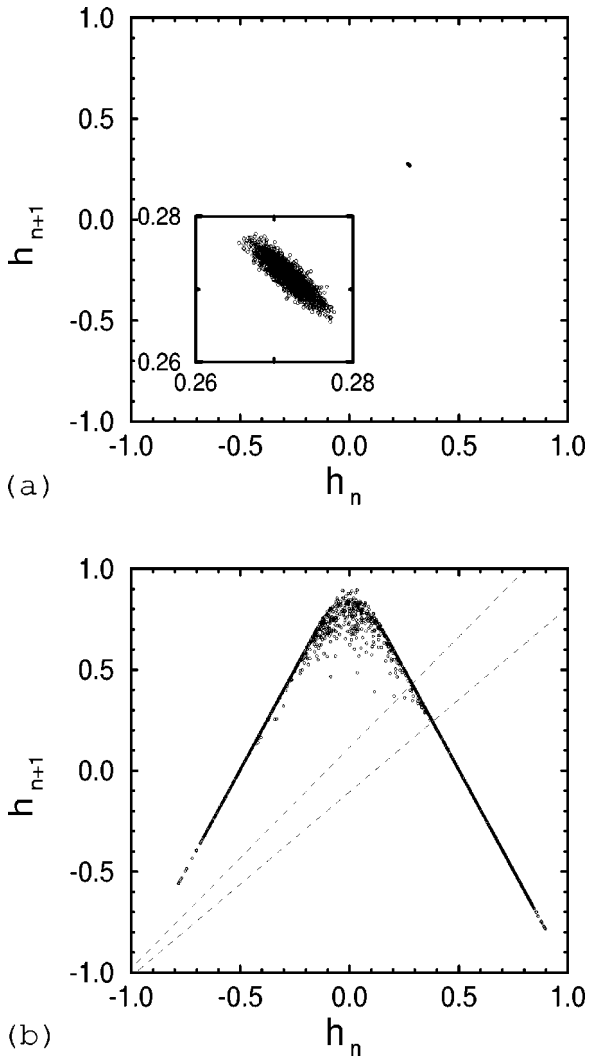

FIG. 1. Return maps of the mean field are shown over 10 000 time steps after 10^5 steps as transient. (a) $a=1.99$, $\epsilon=0.25$, $N=320$. The enlargement is shown in the inset. (b) $a=1.99$, $\epsilon=0.45$, $N=320$. The broken lines represent the criterion (45) in Sec. V.

In the previous paper [33], the numerical calculation of Lyapunov exponents showed that the system (1) has a transition that separates the scattered states into two distinct phases (weak-coupling and strong-coupling phases). In the weak-coupling (strong-coupling) phase, the largest Lyapunov exponent λ_0 decreases (increases) with increasing ϵ for fixed a. The transition is on account of a competition between the local-instability rate λ_{local} and the collective-motion-instability rate Λ. Here, Λ is estimated by the nonlinear Frobenius-Perron equation, which is obeyed by the distribution of the elements in the limit of large size. Λ is expected to give the rate of exponential divergence between two nearby trajectories of the mean-field in the limit of large size. In the weak-coupling phase ($\lambda_{\mathrm{local}}>\Lambda$), the largest Lyapunov exponent obeys the scaling law

$$\lambda_0-\lambda_{\mathrm{local}} \propto \frac{\epsilon}{N}. \tag{6}$$

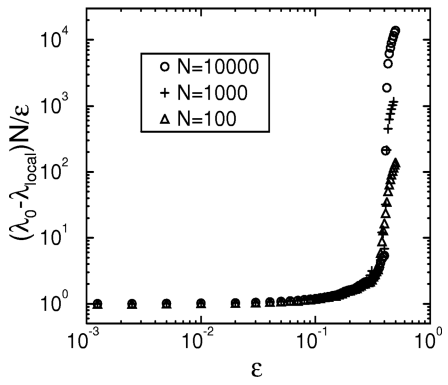

FIG. 2. Log-log plots of the scaled largest Lyapunov exponent $(\lambda_i-\lambda_{\rm local})N/\epsilon$ versus the coupling strength ϵ for three values of system size. The gradient parameter of the map is fixed as $a=1.99$. The largest Lyapunov exponent is obtained from an average over 10^5 steps after discarding 10^5 steps as transient.

On the other hand, in the strong-coupling phase ($\lambda_{\rm local}<\Lambda$), the largest Lyapunov exponent λ_0 approaches the collective-motion-instability rate Λ with increasing N.

III. SCALING LAW OF LYAPUNOV SPECTRUM

In the previous paper, the scaling law (6) for the largest Lyapunov exponent was observed in the weak-coupling phase. We investigate the nature of the Lyapunov exponents in more detail. First, the largest Lyapunov exponent is explored. The scaling law (6) indicates that the difference between the largest Lyapunov exponent λ_0 and the local-instability rate $\lambda_{\rm local}$ is proportional to ϵ and inversely proportional to N. Here, let us consider the scaled largest Lyapunov exponent as $(\lambda_i-\lambda_{\rm local})N/\epsilon$. If the scaling law (6) holds exactly, the scaled largest Lyapunov exponent must be independent of ϵ and N. In Fig. 2, the scaled largest Lyapunov exponent is plotted as a function of ϵ for three values of the system size N and $a=1.99$. Figure 2 shows that, even in the weak-coupling phase ($\epsilon<\epsilon_c\simeq 0.41$ for $a=1.99$ [33]), the deviation from the scaling law (6) increases gradually with increasing coupling strength ϵ. Nevertheless, the scaled largest Lyapunov exponents for three values of system size coincide in the weak-coupling phase. As a result, the relationship

$$\lambda_0-\lambda_{\rm local}\propto\epsilon \tag{7}$$

is valid only in the weak-coupling limit $\epsilon\to 0$. In contrast, the relationship

$$\lambda_0-\lambda_{\rm local}\propto\frac{1}{N} \tag{8}$$

is always valid in the weak-coupling phase region, unless N is too small. In addition, we see from Fig. 2 that the relationship

$$\lambda_0-\lambda_{\rm local}\simeq\frac{\epsilon}{N} \tag{9}$$

holds in the weak-coupling limit $\epsilon\to 0$.

We now investigate the Lyapunov spectrum. Figure 3 shows several examples of the Lyapunov spectra. Figure 3(a) shows the Lyapunov spectra for $\epsilon=0.2$ and several values of a. For all parameters in Fig. 3(a), the systems are in the weak-coupling phase. In Fig. 3(a), all Lyapunov spectra have almost flat shapes. Figure 3(b) shows the Lyapunov spectra for $a=1.99$ and several values of ϵ. For $\epsilon=0.45$, where the system is in the strong-coupling phase, the Lyapunov spectrum has a sharp bend near $i=0$. In the other cases, where the systems are in the weak-coupling phase, Lyapunov spectra have almost flat shapes again. However, the Lyapunov spectra are not degenerate but have a structure obeying a scaling law in the weak-coupling phase, as is seen in the following.

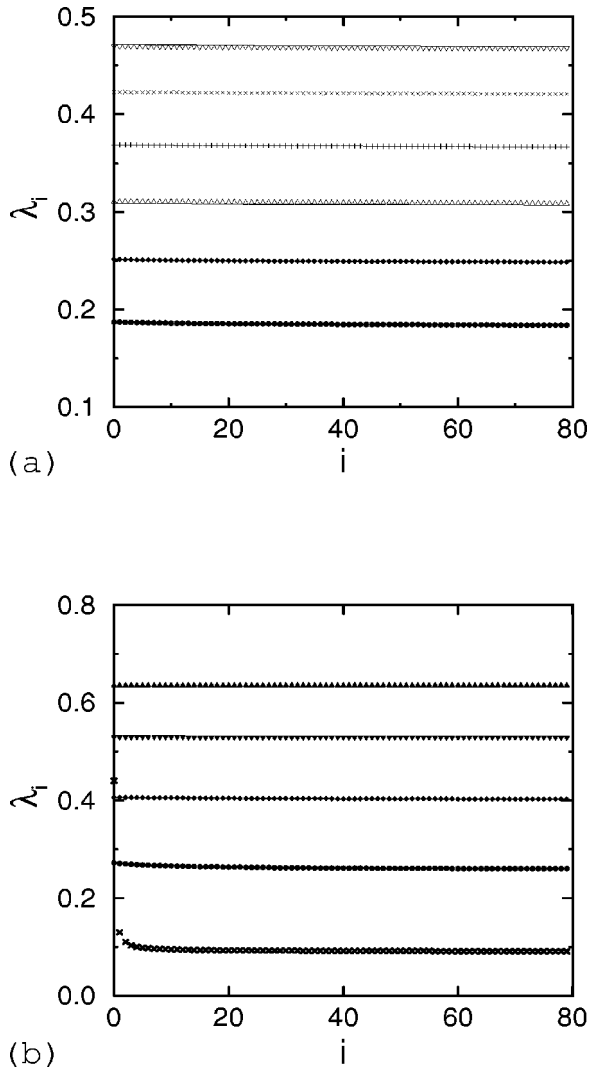

FIG. 3. Lyapunov spectra are plotted for $N=80$. (a) The coupling strength is fixed as $\epsilon=0.2$ and the gradient a is 1.5 (circle), 1.6 (diamond), 1.7 (triangle up), 1.8 (plus), 1.9 (cross), and 1.99 (triangle down). (b) The gradient is fixed as $a=1.99$ and the coupling strength ϵ is 0.05 (triangle up), 0.15 (triangle down), 0.25 (diamond), 0.35 (circle), and 0.45 (cross).

Taking account of Eq. (8), we introduce the scaled Lyapunov spectrum defined as

$$L(i/N)\equiv N(\lambda_i-\lambda_{\rm local}). \tag{10}$$

In Fig. 4, two examples of the scaled Lyapunov spectra are presented for $N=80,160,320$. Figure 4(a) shows that the

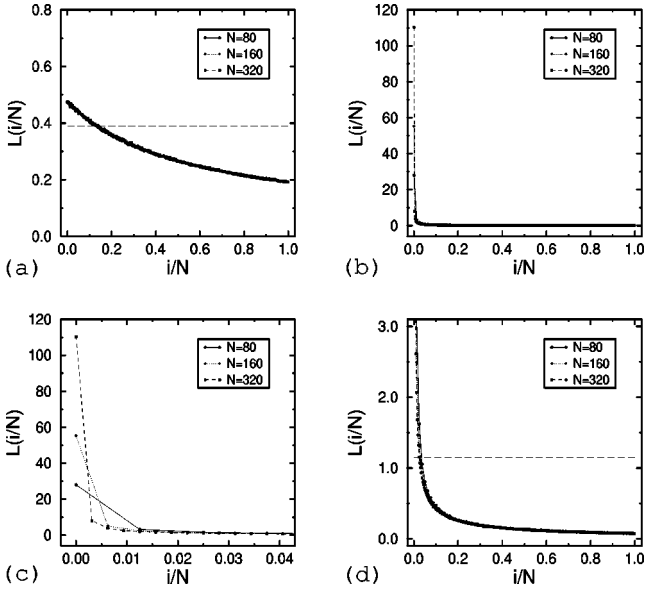

FIG. 4. Scaled Lyapunov spectra are plotted for three values of system size. (a) Weak-coupling phase: $a=1.99$, $\epsilon=0.25$, that is the same parameters as Fig. 1(a). (b) Strong-coupling phase: $a=1.99$, $\epsilon=0.45$, that is the same parameters as Fig. 1(b). (c) The blowup of (b) for the range of $0\leqslant i/N\leqslant 0.05$. (d) The enlargement of (b) for the range of $0\leqslant L(i/N)\leqslant 2$. The lines are to guide the readers' eyes. The horizontal broken lines in (a) and (d) represent the result (39) of the random field approximation.

function $L(i/N)$ is independent of N in the weak-coupling phase. Thus, the Lyapunov exponents can be written in the form

$$\lambda_i=\lambda_{\rm local}+\frac{1}{N}L(i/N;a,\epsilon). \tag{11}$$

Figure 5 shows the scaled Lyapunov spectra for the same parameters as Fig. 3(a). When the gradient a is sufficiently large, $L(x;a,\epsilon)$ appears to be independent of a. Figure 6 shows the scaled Lyapunov spectra for the same parameters as Fig. 3(b). The larger ϵ is, the steeper $L(x;a,\epsilon)$ is. It should be noted that $L(x;a,\epsilon)=0$ for $\epsilon=0$.

On the other hand, in the strong-coupling phase, the scaled Lyapunov spectrum $L(i/N)$ is not independent of N,

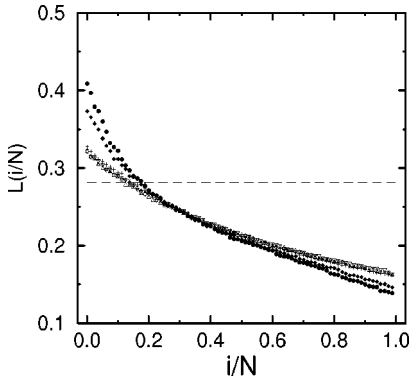

FIG. 5. Scaled Lyapunov spectra are plotted for the same parameters as Fig. 3(a). The horizontal broken line represents the result (39) of the random field approximation. For $a\geqslant 1.7$, the scaled Lyapunov spectra coincide with one curve.

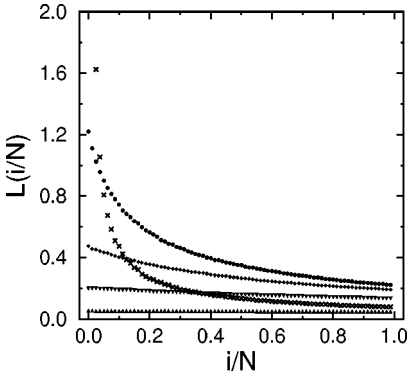

FIG. 6. Scaled Lyapunov spectra are plotted for the same parameters as Fig. 3(b). For $\epsilon=0.45$, the large exponents $[L(0)=28.0$ and $L(1/N)=3.2]$ are not plotted.

as is seen from Figs. 4(b) and 4(c). When the system size N increases, the largest Lyapunov exponent approaches the collective-motion-instability rate Λ, which is larger than $\lambda_{\rm local}$. As a result, $L(0)$ is almost proportional to N. Nevertheless, the scaled Lyapunov spectra $L(i/N)$ coincide with one curve for $i\geqslant 1$ as is seen from Fig. 4(d). Therefore, the Lyapunov exponents except the largest one can be written as

$$\lambda_i=\lambda_{\rm local}+\frac{1}{N}L(i/N;a,\epsilon)\quad (i\geqslant 1). \tag{12}$$

Equation (12) indicates that the scaling law (11) holds except the singularity for the largest one. However, $L(x;a,\epsilon)$ diverges for $x\to 0$ in the strong-coupling phase.

IV. RANDOM FIELD APPROXIMATION

In this section, the theoretical estimation of Lyapunov exponents by the random field approximation is presented. This estimation will disclose the relation between the the Lyapunov exponents and the distribution of the elements $x_t(i)$.

A. Evolution of the tangent vector

Lyapunov exponents can be computed by the linearized dynamics of the tangent vector $\{\xi_t(i)\}$ in the tangent space at $\{x_t(i)\}$ of Eq. (1)

$$\xi_{t+1}(i)=(1-\epsilon)s_t(i)\xi_t(i)+\frac{\epsilon}{N}\sum_{i'=0}^{N-1}s_t(i')\xi_t(i'), \tag{13}$$

where $s_t(i)=-a\,\mathrm{sgn}(x_t(i))$. Thus, the tangent vector at time T is given by

$$\vec{\xi}_T=\left(\prod_{t=0}^{T-1}\mathsf{J}_t\right)\vec{\xi}_0, \tag{14}$$

where J_t is an $N\times N$ Jacobian matrix,

$$\{\mathsf{J}_t\}_{ij}\equiv(1-\epsilon)s_t(i)\,\delta_{ij}+\frac{\epsilon}{N}s_t(i). \tag{15}$$

We define here the multiplier matrix M_T as

$$\mathsf{M}_T = \prod_{t=0}^{T-1} \mathsf{J}_t . \tag{16}$$

The Lyapunov exponents are given as

$$\lambda_i = \lim_{T\to\infty} \frac{1}{2T} \ln \gamma_T^i, \tag{17}$$

where $\gamma_T^i (i=0,1,\ldots,N-1)$ are the N eigenvalues of $\mathsf{M}_T^t \mathsf{M}_T$, where M_T^t is the transpose of M_T. We estimate the multiplier matrix M_T by using the method in [30–32], which is similar to the method used in the theory of directed polymers in a random medium.

B. Assumption

To begin with, the assumption is presented in this subsection. An element $\{\mathsf{M}\}_{ij}$ of the multiplier matrix M_T consists of the sum of the multipliers for all paths connecting $(i,0)$ with $(j,T-1)$ in element-time space. These paths are defined by the functions $i_k(t)$, where k is the index of the path. The multiplier for a certain path k is given by

$$M_k = \left(\frac{\epsilon}{N}\right)^m \left(1-\epsilon+\frac{\epsilon}{N}\right)^{T-m} S_k, \tag{18}$$

where

$$S_k \equiv \prod_{t=o}^{T-1} s_t(i_k(t)). \tag{19}$$

Here m represents the number of integers t that satisfy $i_k(t) \neq i_k(t+1)$ for $0 \leqslant t \leqslant T-1$. Accordingly, m is an integer in $[0,T]$, which depends on path k. Here, let us assume that $s_t(i)$ are random variables as follows:

$$P[s_t(i)=a]=p,$$

$$P[s_t(i)=-a]=1-p, \tag{20}$$

where p describes the skewness of the distribution of the elements. Then, S_k are also random variables, whose probability is given by

$$P(S_k=a^T)=\frac{1+(2p-1)^T}{2},$$

$$P(S_k=-a^T)=\frac{1-(2p-1)^T}{2}. \tag{21}$$

Two random variables S_k and $S_{k'}$ for different paths k and k' are not necessarily independent of each other. To obtain an analytical solution, we assume that S_k for all paths are mutually independent random variables. Consequently, the element of the multiplier matrix M_T is considered as the sum of the mutually independent random variables (18) over all paths.

C. Multiplier matrix

We now estimate the multiplier matrix M_T by using the assumption in the preceding subsection. First, the diagonal elements $\{\mathsf{M}\}_{ii}$ are estimated. A simple calculation of the combination indicates that the total number of paths connecting $(i,0)$ with $(i,T-1)$ for a certain fixed value of m is

$$C_d(m,T)=\left[\frac{(N-1)^m}{N}+\left(1-\frac{1}{N}\right)(-1)^m\right]\frac{T!}{m!(T-m)!}. \tag{22}$$

As a result of Eqs. (18), (21), and (22), there are the number $C_d(m,T)$ of the random variables which are

$$\left(\frac{\epsilon}{N}\right)^m \left(1-\epsilon+\frac{\epsilon}{N}\right)^{T-m} a^T \tag{23}$$

with probability

$$\frac{1+(2p-1)^T}{2} \tag{24}$$

and

$$-\left(\frac{\epsilon}{N}\right)^m \left(1-\epsilon+\frac{\epsilon}{N}\right)^{T-m} a^T \tag{25}$$

with probability

$$\frac{1-(2p-1)^T}{2}. \tag{26}$$

Because of the assumption that they are mutually independent, it is deduced by the central limit theorem that the sum of the above random variables is a random variable that obeys the Gaussian distribution $N(\mu_m,\sigma_m)$ through central limit theorem. Here the average μ_m and the standard deviation σ_m are given by

$$\mu_m = C_d(m,T)\left(\frac{\epsilon}{N}\right)^m \left(1-\epsilon+\frac{\epsilon}{N}\right)^{T-m} a^T (2p-1)^T,$$

$$\sigma_m^2 = C_d(m,T)\left(\frac{\epsilon}{N}\right)^{2m} \left(1-\epsilon+\frac{\epsilon}{N}\right)^{2T-2m} a^{2T}[1-(2p-1)^{2T}]. \tag{27}$$

The diagonal elements $\{\mathsf{M}_T\}_{ii}$ are given by the sum of the variables, each of which obeys the Gaussian distribution $N(\mu_m,\sigma_m)$ from $m=0$ to $m=T$. Because of the nature of Gaussian distribution, $\{\mathsf{M}_T\}_{ii}$ obey the Gaussian distribution $N(\mu_d,\sigma_d)$, where

$$\mu_d = \sum_{m=0}^{T} \mu_m,$$

$$\sigma_d^2 = \sum_{m=0}^{T} \sigma_m^2 . \tag{28}$$

By using the binomial theorem, μ_d and σ_d are described as

$$\mu_d=\frac{1}{N}[a(2p-1)]^T+\left(1-\frac{1}{N}\right)[a(2p-1)(1-\epsilon)]^T,$$

$$\sigma_d^2=\frac{1}{N}a^{2T}\left[\left(1-\epsilon+\frac{\epsilon}{N}\right)^2+\left(\frac{\epsilon}{N}\right)^2(N-1)\right]^T[1-(2p-1)^{2T}],$$

$$+\left(1-\frac{1}{N}\right)a^{2T}\left[\left(1-\epsilon+\frac{\epsilon}{N}\right)^2-\left(\frac{\epsilon}{N}\right)^2\right]^T[1-(2p-1)^{2T}]. \tag{29}$$

Second, we consider the off-diagonal elements $\{\mathsf{M}_T\}_{ij}(i\neq j)$. The total number of the paths connecting $(i,0)$ with $(j,T-1)$ for a certain value of m is

$$C_{\rm od}(m,T)=\left[\frac{(N-1)^m}{N}-\frac{1}{N}(-1)^m\right]\frac{T!}{m!(T-m)!}. \tag{30}$$

From the same calculation as the above one, it is obtained that the off-diagonal elements obey the Gaussian distribution $N(\mu_{\rm od},\sigma_{\rm od})$, where

$$\mu_{\rm od}=\frac{1}{N}[a(2p-1)]^T-\frac{1}{N}[a(2p-1)(1-\epsilon)]^T,$$

$$\sigma_{\rm od}^2=\frac{1}{N}a^{2T}\left[\left(1-\epsilon+\frac{\epsilon}{N}\right)^2+\left(\frac{\epsilon}{N}\right)^2(N-1)\right]^T[1-(2p-1)^{2T}]-\frac{1}{N}a^{2T}\left[\left(1-\epsilon+\frac{\epsilon}{N}\right)^2-\left(\frac{\epsilon}{N}\right)^2\right]^T[1-(2p-1)^{2T}]. \tag{31}$$

D. Results

The results in the preceding subsection indicate that the multiplier matrix is expressed by two matrices as follows.

One of them is the constant matrix A_T given by

$$\{\mathsf{A}_T\}_{ij}=\begin{cases}\dfrac{1}{N}\alpha_1^T+\dfrac{N-1}{N}\alpha_2^T & (i=j),\\ \dfrac{1}{N}\alpha_1^T-\dfrac{1}{N}\alpha_2^T & (i\neq j),\end{cases} \tag{32}$$

where

$$\alpha_1\equiv a(2p-1),$$

$$\alpha_2\equiv a(2p-1)(1-\epsilon). \tag{33}$$

In the case of $p=1$ or $p=0$, which is expected to correspond to the completely synchronized state, the multiplier matrix M_T is expressed by only the constant matrix A_T as $\mathsf{M}_T=\mathsf{A}_T$. Then, the eigenvalues of $\mathsf{M}_T^t\mathsf{M}_T$ are calculated analytically and we obtain $\gamma_T^0=a^{2T}$ and $\gamma_T^i=[a(1-\epsilon)]^{2T}$ $(i\geqslant 1)$. According to Eq. (17), the Lyapunov exponents are obtained as $\lambda_0=\ln a$ and $\lambda_i=\ln[a(1-\epsilon)]$ $(i\geqslant 1)$. These values coincide with the exact solutions in the completely synchronized state.

The other matrix is the random one R_T. The elements $\{\mathsf{R}_T\}_{ij}$ are mutually independent random variables obeying the Gaussian distribution $N(0,1)$. In the case of $0<p<1$, which corresponds to the scattered state, the multiplier matrix M_T is described as

$$\mathsf{M}_T\simeq\mathsf{A}_T+\alpha_3^T\mathsf{R}_T. \tag{34}$$

for large value of T, where

$$\alpha_3\equiv a(1-\epsilon)\sqrt{1+\frac{\epsilon(2-\epsilon)}{N(1-\epsilon)^2}}\ . \tag{35}$$

Here we take into account only the predominant term of Eqs. (29) and (31). Note that α_3 is always larger than $|\alpha_2|$.

When $|\alpha_1|<\alpha_3$, all the elements of the multiplier matrix M_T diverge exponentially as $O(\alpha_3^T)$. Thus, the constant matrix A_T is negligible. The multiplier matrix can be rewritten in the form

$$\mathsf{M}_T\simeq\alpha_3^T\mathsf{R}. \tag{36}$$

When the eigenvalues of $\mathsf{R}^t\mathsf{R}$ are denoted as $\{\gamma_i'\}$, the eigenvalues of $\mathsf{M}_T^t\mathsf{M}_T$ are given by $\alpha_3^{2T}\gamma_i'$. Since the eigenvalues $\{\gamma_i'\}$ are independent of T, we get all the Lyapunov exponents as

$$\lambda_i\simeq\ln\ \alpha_3=\ln\ a+\ln(1-\epsilon)+\frac{1}{2}\ln\left[1+\frac{\epsilon(2-\epsilon)}{N(1-\epsilon)^2}\right]. \tag{37}$$

The random field approximation gives the result that all Lyapunov exponents are degenerate for $|\alpha_1|<\alpha_3$. This N-fold degeneracy agrees with the numerical result that the Lyapunov spectra have almost flat shapes in the weak-coupling phase (see Fig. 3). However, the Lyapunov spectra are not degenerate completely. Thus, this random field approximation does not give the exact shapes of the Lyapunov spectra [see Figs. 4(a) and 5]. The disagreement is due to the assumption that S_k for all paths are mutually independent. In fact, S_k for a path correlates with $S_{k'}$ for another path.

By assuming N is sufficiently large and by using the approximation that $\ln(1+x)\simeq x$ for $x\ll 1$, we rewrite Eq. (37) as

$$\lambda_i \simeq \lambda_{\rm local} + \frac{\epsilon(2-\epsilon)}{2N(1-\epsilon)^2}. \tag{38}$$

Thus, the scaled Lyapunov spectrum is given by

$$L(i/n;a,\epsilon) \simeq \frac{\epsilon(2-\epsilon)}{2(1-\epsilon)^2}. \tag{39}$$

This equation suggests that the scaled Lyapunov spectrum is independent of the system size N. This agrees with the numerical result (11) in the weak-coupling phase. Moreover, Eq. (39) suggests that the scaled Lyapunov spectrum $L(i/n;a,\epsilon)$ does not depend on a. This agrees with the numerical indication that the scaled Lyapunov spectrum is independent of a for sufficiently large a (see Fig. 5). The deviation seen for small values of a may be due to the tendency that the correlation of S_k for different paths increases with decreasing a. Therefore, the scaling law (11) is explained qualitatively by Eq. (38). In addition, in the limit of $\epsilon \to 0$, we obtain Eq. (9) from Eq. (38).

On the other hand, when $|\alpha_1| > \alpha_3$, all the elements of the multiplier matrix M_T diverge exponentially as $\{\mathsf{M}_T\}_{ij} \simeq \alpha_1^T$. As a result, the largest eigenvalue γ_0 also diverges exponentially as $O(\alpha_1^{2T})$. From Eq. (17), we obtain

$$\lambda_0 \simeq \ln|\alpha_1| = \ln a + \ln|2p-1|. \tag{40}$$

Besides, the other eigenvalues γ_i $(i \geqslant 1)$ are still $O(\alpha_3^{2T})$ because $|\alpha_2| < \alpha_3$. Thus, the other Lyapunov exponents λ_i $(i \geqslant 1)$ are given by Eq. (38). This theoretical result explains qualitatively the scaling law (12), which holds except the singularity for the largest Lyapunov exponent. However, as is seen from Fig. 4(d), the exact shape of the scaled Lyapunov spectrum is not obtained either from this random field approximation.

When the system size N is sufficiently large, the approximate value of the largest Lyapunov exponent is given by

$$\lambda_0 \simeq \max(\ln[a|2p-1|], \ln[a(1-\epsilon)]). \tag{41}$$

When $|2p-1| > 1-\epsilon$, λ_0 depends on the skewness p that represents the average probability that the elements have positive values. It is plausible that p is estimated in the form

$$\ln|2p-1| \equiv \lim_{T\to\infty} \frac{1}{T} \sum_{t=0}^{T-1} \ln|2p_t - 1|, \tag{42}$$

where p_t is the fraction of positive elements at time t. When N is an even number, Eq. (42) is divergent if $p_t = 1/2$ at certain time t. However, this divergence is not significant for the Lyapunov exponents because of the contribution from the random matrix R_T. The most simple method to avoid this irrelevant divergence is taking an odd number as N. We use this method when p is estimated. The numerical result for the largest Lyapunov exponent, $\ln[a|2p-1|]$, and $\ln[a(1-\epsilon)]$ are plotted as functions of ϵ for $a = 1.99$ in Fig. 7. As is seen from Fig. 7, the theoretical prediction (41) agrees well with the numerical calculation. The case of $|2p-1| < 1-\epsilon$ corresponds to the weak-coupling phase while the case of $|2p-1| > 1-\epsilon$ corresponds to the strong-coupling phase, as expected. It is evident that there exists a transition near $|2p-1| = 1-\epsilon$. The same type of transition was observed in CML by Pikovsky [31]. Pikovsky denoted as ''variance dominated'' and ''mean dominated'' the weak-coupling and strong-coupling phases, respectively.

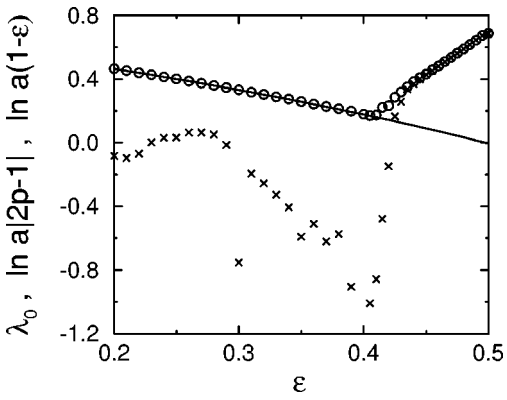

FIG. 7. Comparison between the numerical calculation and the random field approximation (41). The numerical result for the largest Lyapunov exponent of Eq. (1) is plotted for $N = 1000$ (circle). Cross marks represent $\ln[a|2p-1|]$ and the solid line represents $\ln[a(1-\epsilon)]$. When p is calculated, we take $N = 1001$ to avoid the case of $p_t = 1/2$, in which Eq. (42) diverges. $\ln[a|2p-1|]$ is obtained from an average over 10^5 steps as well as λ_0.

In the intermediate region, the theoretical prediction (41) yields considerably smaller values than the numerical results (see Fig. 7). In order to explain this disagreement, we introduce the finite-time average of $|2p_t - 1|$ as

$$\ln q(t;T) \equiv \frac{1}{T} \sum_{t'=t}^{t+T-1} \ln|2p_{t'} - 1|. \tag{43}$$

Figure 8(a) shows the dependence of $q(t;T)$ on time t in the intermediate region for $T = 100$. Obviously, the value of $q(t;T)$ switches between two separated ranges intermittently. Figure 8(b) shows temporal change of the finite-time Lyapunov exponent $\lambda_0(t;T)$ for the same trajectory as Fig. 8(a). As is predicted from Eq. (41), $\lambda_0(t;T) \simeq \ln[a\, q(t;T)]$ during time intervals of $q(t;T) > 1-\epsilon$, whereas $\lambda_0(t;T)$

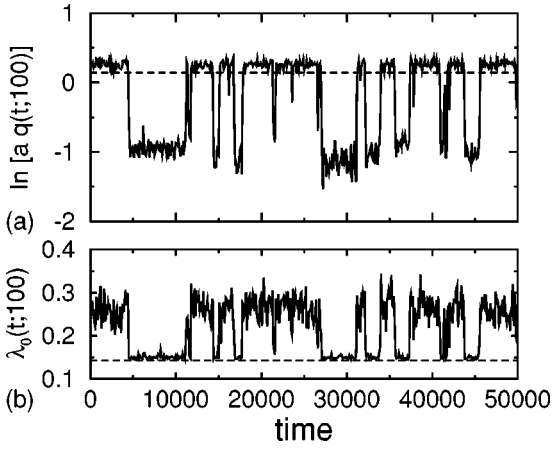

FIG. 8. (a) $\ln[a\, q(t;T)]$ is plotted as a function of t for $a = 1.99$, $\epsilon = 0.42$, $N = 1001$, and $T = 100$. (b) $\lambda_0(t;T)$ is plotted as a function of t for the same trajectory as (a). The horizontal broken line represents $\ln[a(1-\epsilon)] = 0.143\ldots$.

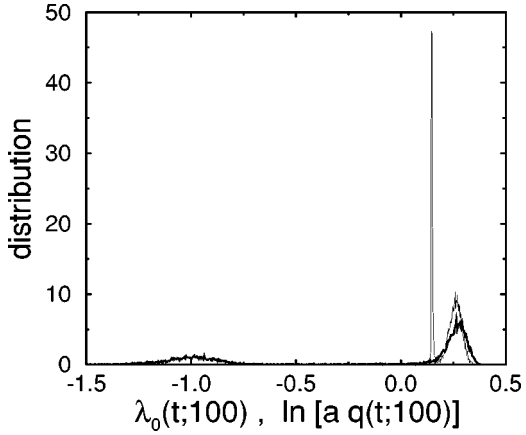

FIG. 9. Comparison between the distributions of $\ln[a\,q(t;T)]$ (thick line) and of the finite-time Lyapunov exponent $\lambda_0(t;T)$ (thin line) for the same parameter as Fig. 8. The bin width is 2^{-8} and the distributions are normalized for their integration to be 1.

$\simeq \ln[a(1-\epsilon)]$ during time intervals of $q(t;T)<1-\epsilon$, Thus, the situation of the strong-coupling phase and that of the weak-coupling phase alternate. In Fig. 9, we show the distributions of $\ln[a\,q(t;T)]$ and $\lambda_0(t;T)$ for the same parameter as Fig. 8. The distribution of $\ln[a\,q(t;T)]$ has two well-defined peaks (thick line in Fig. 9). The lower peak exerts no influence on the finite-time Lyapunov exponent. The higher peak agrees well with a peak of the distribution of the finite-time Lyapunov exponent (thin line). Moreover, the distribution of the finite-time Lyapunov exponent has a sharp peak at $\ln[a(1-\epsilon)]$, as expected.

The distributions of $\ln[a\,q(t;T)]$ for several values of T are shown in Fig. 10. For a sufficiently large value of T, the distribution has only one broad peak. In Fig. 10, the condition $\ln[a\,q(t;T)]<\ln[a(1-\epsilon)]$ is always satisfied when $T=10^5$. In this case, $\lambda_0(t;T=10^5)\simeq\ln[a(1-\epsilon)]$ is expected from the approximate estimation (41). However, there are time intervals where the system behaves as the large-coupling phase, as is seen from the intermittent motion of the finite-time Lyapunov exponent (see Fig. 8). Thus, $\lambda_0(t;T=10^5)$ is considerably larger than the expected value $\ln[a(1-\epsilon)]$. This random field approximation is not always good when T is large.

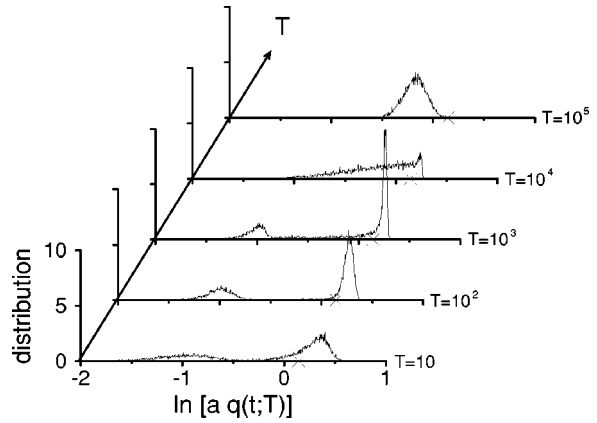

FIG. 10. The distributions of $\ln[a\,q(t;T)]$ for several values of T, $a=1.99$, $\epsilon=0.42$, and $N=1001$. The cross marks represent $\ln[a(1-\epsilon)]$.

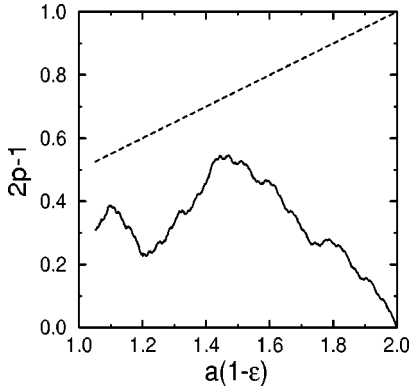

FIG. 11. $2p-1$ is plotted as a function of $a(1-\epsilon)$ if the mean field is constant in the limit of large size. The broken line represents the minimum value of $(1-\epsilon)$. Since the gradient a is in the range $1<a\leqslant 2$, $(1-\epsilon)$ has the minimum value at $a=2$,

V. BAND-STRUCTURE AND TRANSITION

In the preceding section, we have obtained the relation between the Lyapunov exponents and the distribution of the elements. The abrupt transformation of the distribution takes place when chaotic bands are broken through tangent bifurcation, as we see in the following.

To begin with, we assume that the mean field is constant. Thus, the system has 2^n chaotic bands when $2^{2^{-n+1}}<a(1-\epsilon)<2^{2^{-n}}$. In the limit of large size, the distribution function defined by

$$\rho_t(x)=\lim_{N\to\infty}\frac{1}{N}\sum_{i=0}^{N-1}\delta(x-x_t(i)) \tag{44}$$

is a constant function that consists of 2^n separated supports. When $\epsilon=0$, this can be the case. Since p_t is also independent of the time step t, the skewness p is determined by only the value of $a(1-\epsilon)$. Under the above assumption, $|2p-1|$ is smaller than $1-\epsilon$ for any value of $a(1-\epsilon)$, as is seen from Fig. 11.

However, the real values of $|2p-1|$ are different from the values shown in Fig. 11 when $\epsilon\neq 0$. This is because neither the mean field nor the distribution function is constant. Three successive snapshots of $\rho_t(x)$ are shown in Fig. 12. When the two-band structure is retained [Fig. 12(a)], the time series of p_t is limited in a small domain. Thus, it is expected that $|2p-1|$ is not over $1-\epsilon$. On the other hand, when the two-band structure is broken [Fig. 12(b)], the distribution function has only one narrow support, which fluctuates chaotically. Thus, p_t often takes 1 or -1. Accordingly, $|2p-1|$ can exceed $1-\epsilon$. As an example, we consider the intermittent behavior shown in Fig. 8. The temporal change of the distribution of $x_t(i)$ is displayed in Fig. 13. During time intervals where the system behaves as the weak-coupling phase, two chaotic bands are observed (compare Figs. 8 and 13). On the other hand, no band structure is observed during time intervals where the system behaves as the strong-coupling phase. Figure 13 suggests that the intermittent switching between the above two situations is due to the creation and the extinction of two-band structure.

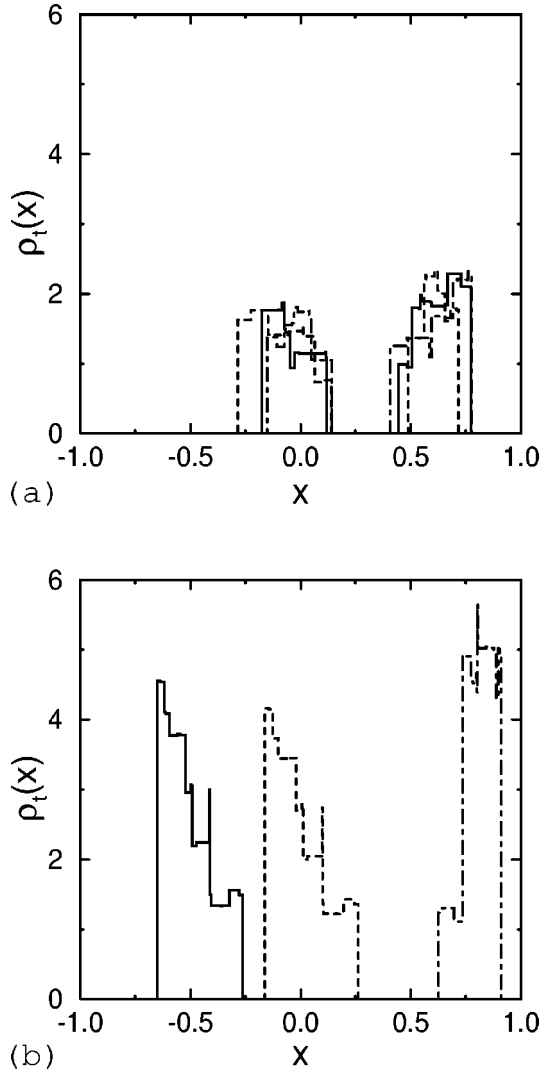

FIG. 12. The three successive snapshots of $\rho_t(x)$ are shown in order as solid, dashed, and dot-dashed lines; (a) two-band structure is retained for $a=1.99, \epsilon=0.35$; (b) two-band structure is broken for $a=1.99, \epsilon=0.45$. The distribution functions $\rho_t(x)$ are calculated by the nonlinear Frobenius-Perron equation.

Although there are also more than two band attractors, we focus on the two-band structure in the following. This is because the two-band structure is significant for Lyapunov exponents, besides which more than two bands are rarely seen. To explore the two-band structure, we consider the two-iterated map $F_{t+1}(F_t(x))$, where $F_t(x)$ was given by Eq. (4). The shape of $F_{t+1}(F_t(x))$ is determined by h_t and h_{t+1}. Two illustrations of the two-iterated maps for $a(1-\epsilon)<\sqrt{2}$ are given in Fig. 14. In Fig. 14(a), the two-iterated map has three unstable fixed points. Thus, two chaotic bands exist and the elements in the two different bands are separated by the middle unstable fixed point. On the other hand, there is only one unstable fixed point in Fig. 14(b). In this case, one of the two chaotic bands is extinguished through a tangent bifurcation. The two bands of the two-iterated map are retained on the condition that the successive pair (h_t, h_{t+1}) of the mean-field satisfy the following two equations:

$$(1-\epsilon)[1-a(1-\epsilon+\epsilon h_t)]+\epsilon h_{t+1}<0,$$

$$(1-\epsilon)[1-a(1-\epsilon+\epsilon h_{t+1})]+\epsilon h_t<0, \qquad (45)$$

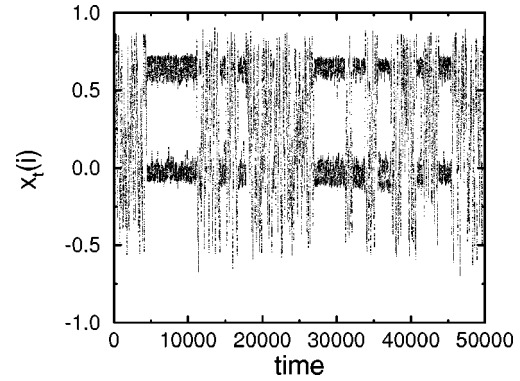

FIG. 13. The temporal change of the distribution of $x_t(i)$ for the same trajectory as Fig. 8. $x_t(i)$ are plotted for $i=0,1,2,\ldots 99$ at every 100 time step.

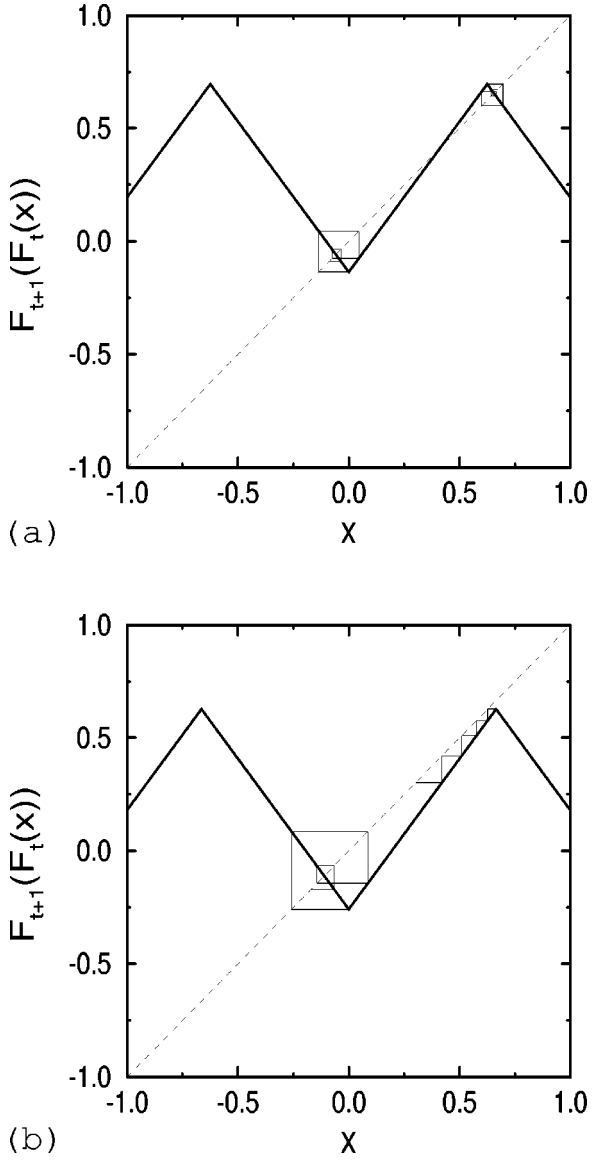

FIG. 14. The two-iterated maps $F_{t+1}(F_t(x))$ at $t=11\,100$ and $t=11168$ for the same trajectory as Fig. 8 are shown. The thin lines are trajectories starting from apices.

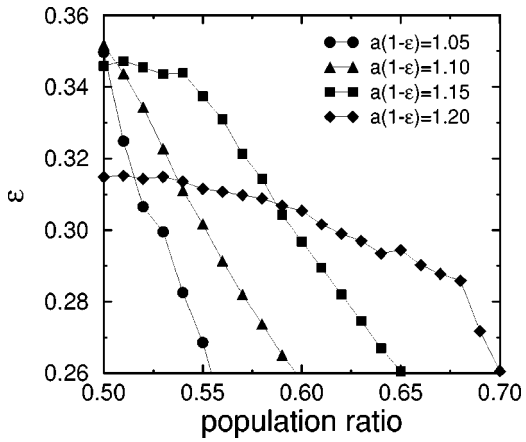

FIG. 15. The coupling strength ϵ beyond which the two bands are broken is plotted as a function of the population ratio between the two bands. We numerically calculate by averaging over 20 realizations where ϵ increases by 0.0001 every 10^6 time steps for the system of $N=100$. The lines are to guide the readers' eyes.

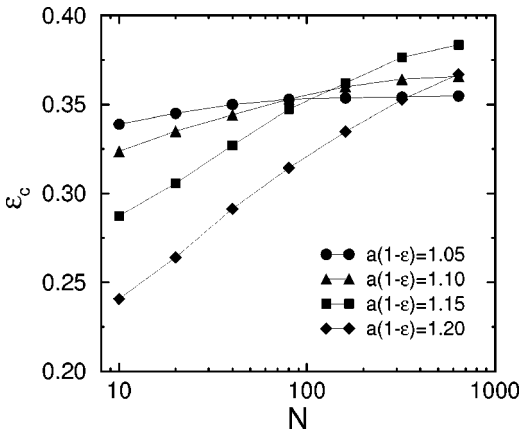

FIG. 16. The critical coupling ϵ_c is plotted as a function of the system size N, where the initial condition is the two-band-structure whose population ratio is 1/2. We calculate in the same way as Fig. 15. The lines are to guide the readers' eyes.

when $a(1-\epsilon)<\sqrt{2}$. In Fig. 1(b), the criterion (45) is displayed as the region between the two broken lines. In the strong-coupling phase, the criterion (45) is satisfied at some time steps but broken at the other time steps. Thus, the criterion (45) is not a sufficient condition for the two-band structure to exist in the model (1).

Taking into account the fact that the bifurcation structure of the model (1) depends on $a(1-\epsilon)$ in a rugged way (see Fig. 11 and [20,23]), it is desirable that the value of $a(1-\epsilon)$ be fixed in order to study the transition. Thus, we consider the situation in which ϵ increases progressively with fixed $a(1-\epsilon)$. When two-band structure is retained, the number of elements in each band is constant. Thus, there exist a lot of two-band states that are characterized by the population (N_1,N_2) of the elements in each band. To distinguish these states, we define the population ratio as $\max(n_1,n_2)$, where $n_1=N_1/N$, $n_2=N_2/N$, and $n_1+n_2=1$. The coupling strength beyond which the two-band state is unstable depends on the population ratio (Fig. 15). The two-band state with the population ratio 1/2 is the most stable, as is seen from Fig. 15. Let ϵ_c denote the coupling strength at which the two-band state with population ratio 1/2 loses the stability. Thus, there is no stable two-band structure above the critical coupling ϵ_c. The critical coupling ϵ_c increases with the system size N (see Fig. 16). This is due to the finite-size effect that the fluctuation of the mean field decreases with the system size. For some values of $a(1-\epsilon)$, the critical coupling ϵ_c appears to saturate [the cases of $a(1-\epsilon)=1.05,1.10,1,15$ in Fig. 16]. Thus, the transition exists in the limit of large size. On the other hand, there are values of $a(1-\epsilon)$ where the two-band structure is always retained for sufficiently large system size in the range of $1<a\leqslant 2$ and $\epsilon>0$ [the case of $a(1-\epsilon)=1.20$ in Fig. 16].

The order parameter H is defined as the fraction of the time steps when Eq. (45) is not fulfilled. If $H=0$, the distribution function is always two-band. Figure 17 shows H when ϵ increases progressively with fixed $a(1-\epsilon)$. Here, the initial condition is selected that the population ratio be 1/2 for $\epsilon=0.2$. For small values of $a(1-\epsilon)$ [Fig. 17(a)], the change of H has a clear jump. In this case, a hysteresis is observed, as seen from the dashed line in Fig. 17(a). On the other hand, for large values of $a(1-\epsilon)$, neither jump nor hysteresis is observed [see Figs. 17(b), 17(c), and 17(d)]. Even in the region where all two-band states are unstable, the system can spend long stretches of time being a two-band state. Thus, the intermittent behavior seen in Fig. 8 exists in the wide parameter region. As a result, H changes gradually.

In order to characterize the intermittent behavior, we calculate the probability of temporary two-band states of duration τ. Let $D(\tau)$ denote the distribution probability of the duration τ, which is measured by using the criterion (45). Even when no temporary two-band state is observed, (h_t,h_{t+1}) often enters in the region described by Eq. (45). In the region (45), the rate of the exponential divergence for the

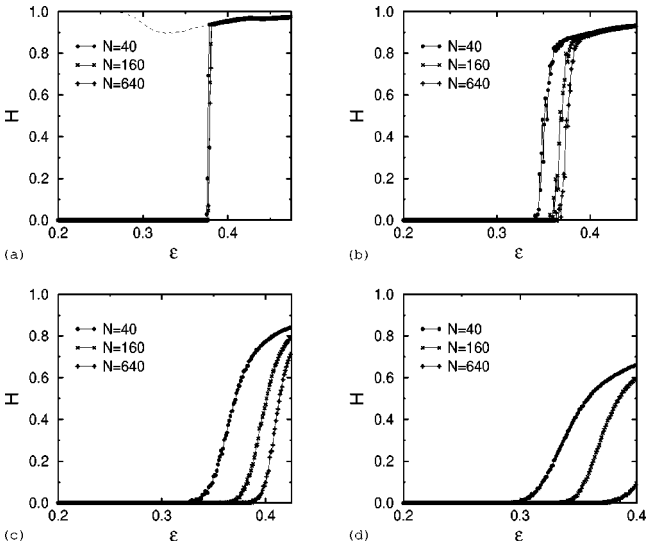

FIG. 17. The order parameter H is plotted as a function of ϵ for three values of system size. The order parameter H is averaged over 20 realizations where ϵ increases by 0.0001 every 10^6 time steps. The initial condition is selected that the population ratio is 1/2 at $\epsilon=0.2$. (a) $a(1-\epsilon)=1.05$; (b) $a(1-\epsilon)=1.10$; (c) $a(1-\epsilon)=1.15$; (d) $a(1-\epsilon)=1.20$. In (a), the dashed line represents the order parameter H when ϵ decreases for $N=160$. This dashed line is not shown in (b), (c), and (d), because no hysteresis is observed.

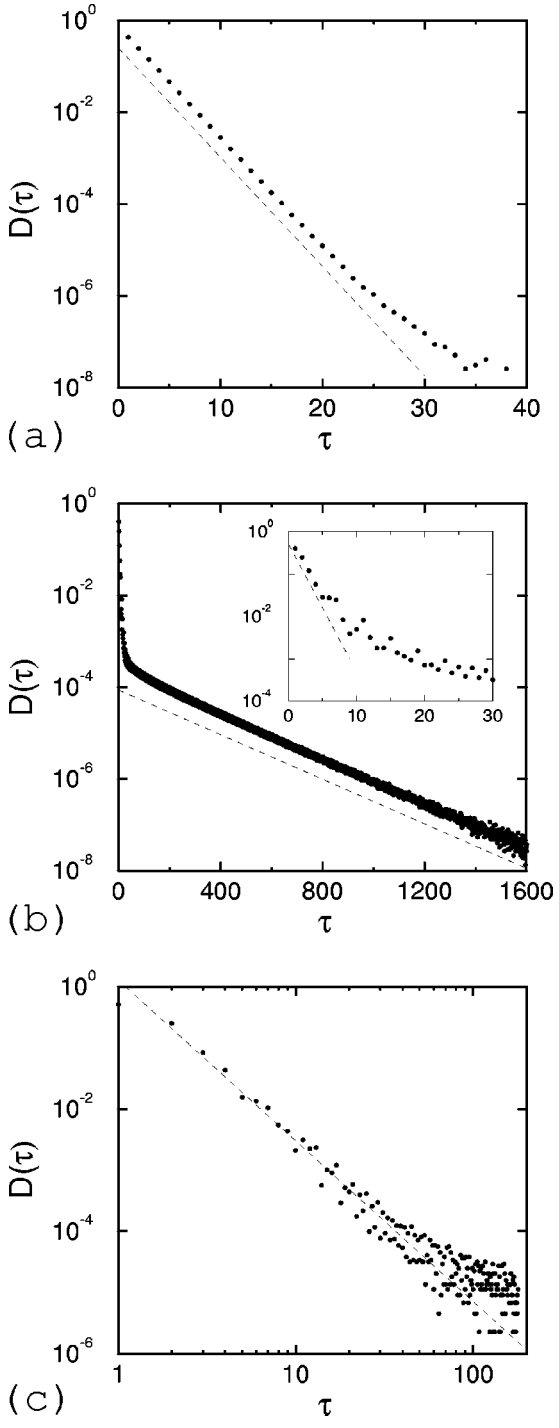

FIG. 18. The distributions $D(\tau)$ of the length τ during which the criterion (45) is retained. The distributions are calculated from a trajectory over 10^{10} time steps. (a) Linear-log plotting for the case that no two-band structure is observed: $a=1.75$, $\epsilon=0.4$ [$a(1-\epsilon)=1.05$], $N=160$. The distribution probability has exponential decay as $D(\tau)\propto a^{-\tau}$. The broken line represents an exponential decay with rate a. (b) Linear-log plotting for the case in which intermittent behavior is observed: $a=2$, $\epsilon=0.4$ [$a(1-\epsilon)=1.2$], $N=160$. There is another exponential decay with a considerably smaller decay rate. The broken line represents an exponential decay with rate 1.006. The blowup is shown in the inset. The broken line in the inset represents an exponential decay with rate a. (c) Log-log plotting for the case of $\epsilon=0.335\sim\epsilon_c$ when $a(1-\epsilon)=1.20$ and $N=160$. The dashed line represents the fitting power law with an exponent $-2.63\ldots$.

mean field is given by a approximately [refer to Fig. 2(b)]. Thus, the distribution probability $D(\tau)$ is expected to have the exponential decay as $D(\tau)\propto a^{-\tau}$. The numerical result agrees well with this expectation [Fig. 18(a)]. This fast exponential decay is not relevant to the intermittent behavior. On the other hand, when the intermittent behavior is observed, a slow exponential decay also exists in $D(\tau)$ [Fig. 18(b)]. Thus, the probability of the duration of the temporary two-band states decays exponentially. This result indicates that the temporary two-band state has a characteristic time, which is longer than the time scale of the individual chaotic elements. This characteristic time increases when ϵ decreases. Since for $\epsilon<\epsilon_c$ two-band states became attractors, this characteristic time is expected to diverge at ϵ_c. In the neighborhood of ϵ_c, the distribution probability $D(\tau)$ obeys a power law, as is seen from Fig. 18(c). In Fig. 18(c), the deviation from the power law is seen when $\tau\sim 1$. It is because there is also the exponential decay, which is irrelevant to the intermittent behavior. The preliminary calculation suggests that the exponent of the power law depends on the $a(1-\epsilon)$ but is independent of N. However, there is a limit in the approach using the criterion (45), because this criterion is not a sufficient condition in which temporary two-band states can exist. A different approach would be required to study the critical phenomena and the universality classes of the transitions in detail.

VI. CONCLUSION

We have investigated the Lyapunov spectra in globally coupled tent maps. There are two phases in the scattered region, where the completely synchronized state is unstable. In the weak-coupling phase, the Lyapunov spectra obey the scaling law (11) with varying N. The strong-coupling phase is seen between the weak-coupling and the completely synchronized states. Even in the strong-coupling phase, the scaling law holds except for the singularity of the largest Lyapunov exponent. We note here that the scaling law is not always clear in a medium region between the weak-coupling and strong-coupling phases. This is due to the intermittent behavior (Fig. 8) and the dependence of the critical coupling ϵ_c on the system size N (Figs. 16 and 17).

The theoretical calculation by the random field approximation explained qualitatively the nature of the Lyapunov spectra. This study demonstrated that the skewness p [or $q(t;T)$] of the distribution of the elements is important to the Lyapunov exponents. The exact shape of the scaled Lyapunov spectrum $L(x;a,\epsilon)$ was not given by this random field approximation. The correlation between the elements is considered only through the skewness p. The exact shape of $L(x;a,\epsilon)$ may be determined by the correlation, which was ignored in our approximation.

The largest Lyapunov exponent was estimated as Eq. (41) for sufficiently large system size. This result indicated there is a transition. In the previous paper [33], this transition was investigated in terms of the competition between the local-instability rate $\lambda_{\rm local}$ and the collective-motion-instability rate Λ. In this paper, the random field approximation showed that this transition is also due to the competition between the random matrix term $\alpha_3^T \mathsf{R}_T$ and the constant one A_T. Apparently, the elements of the random matrix $\alpha_3^T \mathsf{R}_T$ are given as

$\pm\exp(\lambda_{\mathrm{local}})$ for $N\to\infty$. Thus, the matrix A_T is expected to be relevant to the collective-motion-instability-rate Λ. While in the weak-coupling phase the largest Lyapunov exponent depends only on the system parameters, in the strong-coupling phase it depends also on the skewness p.

We characterized the intermittent switching between the two phases by introducing the finite-time average of $|2p_t-1|$. This intermittent switching is due to tangent bifurcations due to the temporal change of the mean field. This tangent bifurcation is explained well by using the two-iterated map. ''Internal'' bifurcations such as this have been studied in connection with the quasiperiodic collective motion in globally coupled logistic maps by Shibata and Kaneko [22]. The intermittent behavior is observed even in the limit of large size. The temporary two-band state has a characteristic time. The characteristic time depends on the parameters a, ϵ, and N.

Furthermore, we explored the transition in terms of two-band structure of the two-iterated map. Continuous and discontinuous transitions were observed. In the case of the continuous transition, the transition point depends on the system size. Near the transition point, there is a power law in the probability of the duration of the temporary two-band states. Recently the nonequilibrium transitions in high-dimensional chaos have been investigated in connection with phase transitions in equilibrium systems [34–41]. There are several coupled nonlinear systems that show the clear critical properties [5,26,34–39]. The investigation of the critical properties for our transition is now progress. On the other hand, in the case of small $a(1-\epsilon)$ [Fig. 17(a)], we had a discontinuous transition. Discontinuous phase transitions such as this have been reported for some coupled nonlinear systems [40,41]. Our transition is complicated because the weak-coupling phase has a lot of ''macroscopic'' separated states depending on the population ratio of two separated bands. In addition, since the concept of space loses meaning for global coupling, the correlation between any two elements should never be ignored. In order to understand clearly the critical phenomena of the transition for the globally coupled systems, more research would be required.

ACKNOWLEDGMENTS

The author appreciates Y. Kuramoto, T. Chawanya, K. Kaneko, T. Shibata, S. Sasa, S. Kitsunezaki, N. Nakagawa, and T. Mizuguchi for their support. The author would like to thank K. Kawamura as well as others from the staff of the ''Research for the Future'' Project in Keio University.

[1] K. Ikeda and K. Matsumoto, J. Stat. Phys. **44**, 955 (1986).
[2] R. Livi, A. Politi, S. Ruffo, and A. Vulpiani, J. Stat. Phys. **46**, 147 (1987).
[3] M. Yamada and K. Ohkitani, Phys. Rev. Lett. **60**, 983 (1988).
[4] S. Isola, A. Politi, S. Ruffo, and A. Torcini, Phys. Lett. A **143**, 365 (1990).
[5] H. Chaté, Europhys. Lett. **21**, 419 (1993).
[6] N. Nakagawa and Y. Kuramoto, Physica D **80**, 307 (1995).
[7] T. Bohr, G. Grinstein, and C. Jayaprakash, Chaos **5**, 412 (1995).
[8] K. Kaneko, Physica D **41**, 137 (1990).
[9] K. Kaneko, *Theory and Applications of Coupled Map Lattice* (John Willey & Sons, New York, 1993).
[10] K. Kaneko, Phys. Rev. Lett. **65**, 1391 (1990).
[11] K. Kaneko, Physica D **55**, 368 (1992).
[12] G. Perez and H.A. Cerdeira, Phys. Rev. A **46**, 7492 (1992).
[13] A.S. Pikovsky and J. Kurths, Physica D **76**, 411 (1994).
[14] A.S. Pikovsky and J. Kurths, Phys. Rev. Lett. **72**, 1644 (1994).
[15] M.G. Cosenza, Phys. Lett. A **204**, 128 (1994).
[16] K. Kaneko, Physica D **86**, 158 (1995).
[17] W. Just, J. Stat. Phys. **79**, 429 (1995).
[18] S.V. Ershov and A.B. Potapov, Physica D **86**, 523 (1995).
[19] S. Morita, Phys. Lett. A **211**, 258 (1996).
[20] T. Chawanya and S. Morita, Physica D **116**, 44 (1998).
[21] T. Shibata and K. Kaneko, Europhys. Lett. **38**, 417 (1997).
[22] T. Shibata and K. Kaneko, e-print chao-dyn/9802018.
[23] N. Nakagawa and T.S. Komatsu, Phys. Rev. E **57**, 1570 (1998).
[24] T. Bohr, G. Grinstein, Yu He, and C. Jayaprakash, Phys. Rev. Lett. **58**, 2155 (1987).
[25] H. Chaté and P. Manneville, Europhys. Lett. **17**, 291 (1992).
[26] H. Chaté, A. Lemaître, Ph. Marcq and P. Manneville, Physica A **224**, 447 (1996).
[27] D. Domínguez and H. A. Cerdeira, Phys. Rev. Lett. **71**, 3359 (1993).
[28] N. Nakagawa and Y. Kuramoto, Physica D **75**, 74 (1993).
[29] M.L. Chabanol, V. Hakim, and W.J. Rappel, Physica D **103**, 273 (1997).
[30] R. Livi, A. Politi, and S. Ruffo, J. Phys. A **25**, 4813 (1992).
[31] A.S. Pikovsky, Chaos **3**, 225 (1993).
[32] F. Cecconi and A. Politi, Phys. Rev. E **56**, 4998 (1997).
[33] S. Morita, Phys. Lett. A **226**, 172 (1997).
[34] J. Miller and D.A. Huse, Phys. Rev. E **48**, 2528 (1993).
[35] H. Sakaguchi, Phys. Lett. A **180**, 235 (1993).
[36] J. Losson, J. Milton, and M.C. Mackey, Physica D **81**, 177 (1995).
[37] Ph. Marcq, H. Chaté, and P. Manneville, Phys. Rev. Lett. **77**, 4003 (1996).
[38] C.S. O'Hern, D.A. Egolf, and H.S. Greenside, Phys. Rev. E **53**, 3374 (1996).
[39] D.A. Egolf and H.S. Greenside, Phys. Rev. Lett. **74**, 1751 (1995).
[40] H. Chaté, Europhys. Lett. **6**, 591 (1988).
[41] R. Müller, K. Lippert, A. Kühnel, and U. Beln, Phys. Rev. E **56**, 2658 (1997).